Time-shift imaging condition

Paul Sava and Sergey Fomel, Bureau of Economic Geology, The University of Texas at Austin

SUMMARY

We derive a new generalized imaging condition based on time shifts between source and receiver wavefields. This imaging condition contrasts with other imaging techniques requiring space shifts between the two wavefields. This imaging condition is applicable to both Kirchhoff and wave-equation migrations. The transformation allows us to generate common-image gathers presented as function of either time-shift or pseudo-angle at every location in space. Inaccurate migration velocity is revealed by common-image gathers with non-flat events.

INTRODUCTION

A key challenge for imaging in complex areas is accurate determination of a velocity model that describes with sufficient precision wave propagation in the area under investigation. Migration velocity analysis is based on image accuracy indicators that are optimized when data are correctly imaged. A common procedure for velocity analysis is based on alignment of images created with multi-offset data. An optimal choice of image analysis can be done in the angle domain which is free of some of the complicated artifacts present in offset gathers in complex areas (Stolk and Symes, 2002).

Migration velocity analysis after migration by wavefield extrapolation requires image decomposition function of scattering angles relative to reflector normals. Several methods have been proposed for such decompositions (de Bruin et al., 1990; Xie and Wu, 2002; Prucha et al., 1999; Mosher and Foster, 2000; Rickett and Sava, 2002; Sava and Fomel, 2003; Soubaras, 2003; Biondi and Symes, 2004). These procedures require decomposition of extrapolated wavefields in components that are related to the reflection angle.

A key component of such image decompositions is the imaging condition. A careful implementation of this imaging condition preserves all information necessary to decompose images in their angle-dependent components. The challenge is not only to use these angle-dependent images for velocity or amplitude analysis, but also to construct them cheaply, reliably and with direct access to velocity information.

This paper presents a different form of imaging condition. The key idea of this new imaging condition is to use time-shifts instead of space-shifts between wavefields computed from sources and receivers. This imaging concept is applicable to both Kirchhoff migration and migration by wavefield extrapolation. We present a brief theoretical analysis of this new imaging condition, followed by examples illustrating the main features of this new technique.

IMAGING CONDITION IN WAVE-EQUATION MIGRATION

No shift imaging condition

A traditional imaging condition for shot-record migration, also known as $U\overline{D}$ imaging condition (Claerbout, 1985), consists of time cross-correlation at every image location between the source and receiver wavefields, followed by image extraction at zero time:

$$\mathbf{u}(\mathbf{m},t) = \mathbf{u}_s(\mathbf{m},t) \star \mathbf{u}_r(\mathbf{m},t) \ , \tag{1}$$

$$\mathbf{R}(\mathbf{m}) = \mathbf{u}(\mathbf{m},t=0) \ . \tag{2}$$

Here, $\mathbf{m} = [m_x, m_y, m_z]$ is a vector describing the locations of image points, $\mathbf{u}_s(\mathbf{m},t)$ and $\mathbf{u}_r(\mathbf{m},t)$ are source and receiver wavefields respectively, and $\mathbf{R}(\mathbf{m})$ denotes the migrated image. The symbol $\star$ denotes cross-correlation in time.

Space-shift imaging condition

Another generalized imaging condition (Sava and Fomel, 2005) estimates image reflectivity using the expressions:

$$\mathbf{u}(\mathbf{m},\mathbf{h},t) = \mathbf{u}_s(\mathbf{m}-\mathbf{h},t) \star \mathbf{u}_r(\mathbf{m}+\mathbf{h},t) \ , \tag{3}$$

$$\mathbf{R}(\mathbf{m},\mathbf{h}) = \mathbf{u}(\mathbf{m},\mathbf{h},t=0) \ . \tag{4}$$

Here, $\mathbf{h} = [h_x, h_y, h_z]$ is a vector describing the local source-receiver separation in the image space. Special cases of this imaging condition were presented by Rickett and Sava (2002) for horizontal space-shift, and by Biondi and Symes (2004) for vertical space-shift.

Angle-domain common-image gathers can be obtained by a simple slant-stack operation on migrated images:

$$\mathbf{R}(\mathbf{m},\mathbf{h}) \Longrightarrow \mathbf{R}(\mathbf{m},\tan\theta) \ , \tag{5}$$

where $\tan\theta$ is the dimensionless slant-stack parameter.

Time-shift imaging condition

Another possible imaging condition involves cross-correlation of the source and receiver wavefields in time, as opposed to space:

$$\mathbf{u}(\mathbf{m},t,\tau) = \mathbf{u}_s(\mathbf{m},t-\tau) \star \mathbf{u}_r(\mathbf{m},t+\tau) \ , \tag{6}$$

$$\mathbf{R}(\mathbf{m},\tau) = \mathbf{u}(\mathbf{m},\tau,t=0) \ . \tag{7}$$

Here, τ is a time shift between the source and receiver wavefields prior to imaging. This imaging condition can be implemented in the Fourier domain using the expression

$$\mathbf{R}(\mathbf{m},\tau) = \sum_{\omega} \mathbf{U}_s(\mathbf{m},\omega) \overline{\mathbf{U}_r(\mathbf{m},\omega)} e^{2i\omega\tau} \ , \tag{8}$$

which simply involves a phase-shift applied to the wavefields prior to summation over frequency ω for imaging at zero time. The over-line represents a complex conjugate applied on the receiver wavefield $\mathbf{U}_r$ in the Fourier domain.

Pseudo angle-domain common-image gathers can be obtained by a simple slant-stack operation on migrated images:

$$\mathbf{R}(\mathbf{m},\tau) \Longrightarrow \mathbf{R}(\mathbf{m},\nu) \ , \tag{9}$$

where ν is the slant-stack parameter with velocity units.

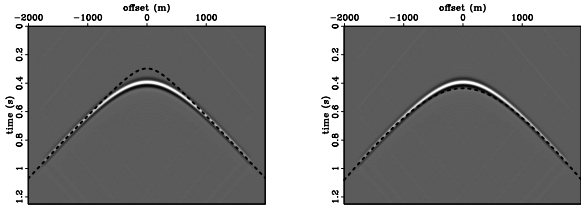

Figure 1: An image is formed when the Kirchoff stacking curve (dashed line) touches the true reflection response. Left: the case of under-migration; right: over-migration.

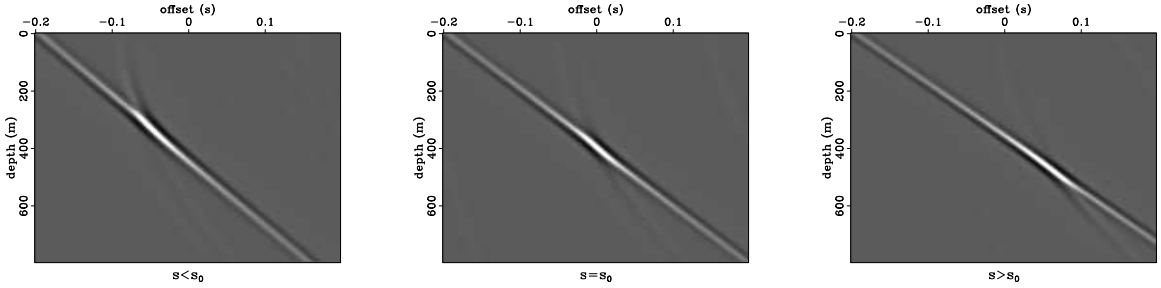

Figure 2: Common-image gathers for time-shift imaging.

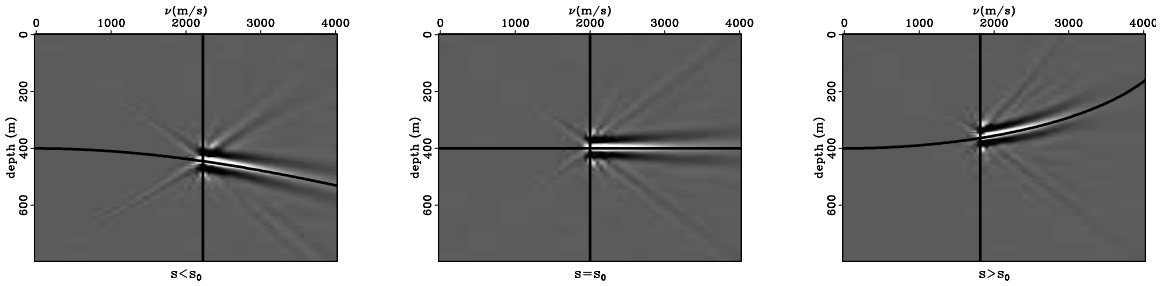

Figure 3: Common-image gathers after slant-stack in time-offset. ν is the slant-stack parameter in the $\{\mathbf{m},\tau\}$ space. The vertical line indicates the migration velocity.

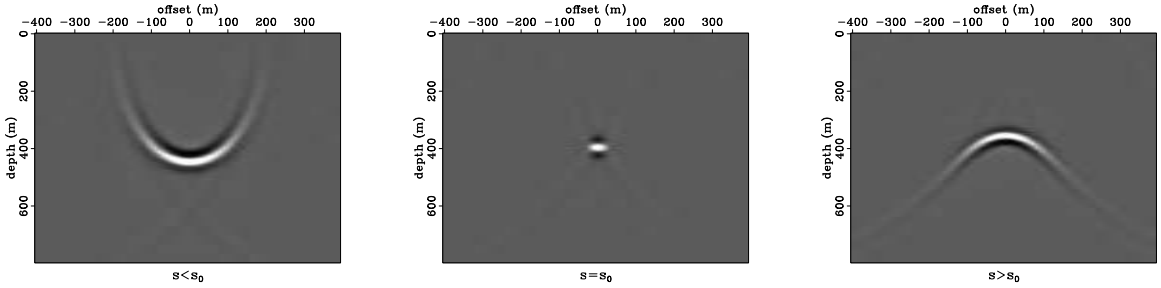

Figure 4: Common-image gathers for space-shift imaging.

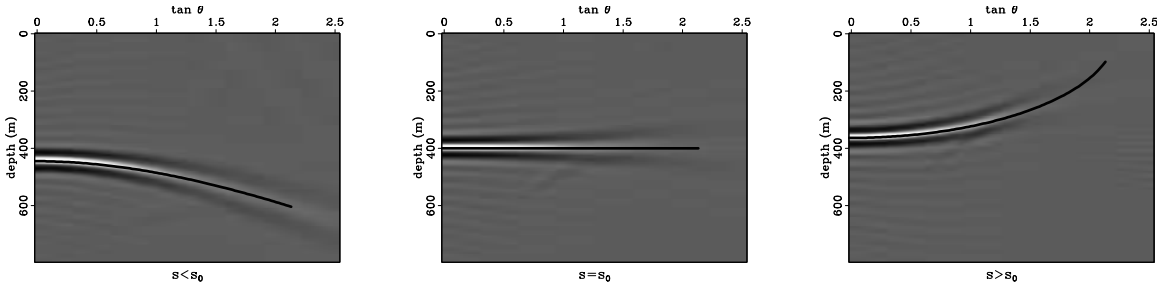

Figure 5: Common-image gathers after slant-stack in space-offset. $\tan\theta$ is the slant-stack parameter in the $\{\mathbf{m},\mathbf{h}\}$ space.

IMAGING CONDITION IN KIRCHHOFF MIGRATION

The imaging condition described in the preceding section has an equivalent formulation in Kirchhoff imaging. Traditional construction of common-image gathers using Kirchhoff migration is represented by the expression

$$\mathbf{R}\left(\mathbf{m},\widehat{\mathbf{h}}\right)=\sum_{\widehat{\mathbf{m}}}\widehat{\mathbf{u}}\left[\widehat{\mathbf{m}},\widehat{\mathbf{h}},T_s\left(\mathbf{m},\widehat{\mathbf{m}}-\widehat{\mathbf{h}}\right)+T_r\left(\mathbf{m},\widehat{\mathbf{m}}+\widehat{\mathbf{h}}\right)\right]\ , \qquad (10)$$

where $\widehat{\mathbf{u}}\left(\widehat{\mathbf{m}},\widehat{\mathbf{h}},t\right)$ is the recorded wavefield at the surface as a function of surface midpoint and offset, $\widehat{\mathbf{m}}$ and $\widehat{\mathbf{h}}$. T_s and T_r stand for traveltime from sources and receivers at coordinates $\widehat{\mathbf{m}}-\widehat{\mathbf{h}}$ and $\widehat{\mathbf{m}}+\widehat{\mathbf{h}}$ to points in the subsurface at coordinates $\mathbf{m}$. For simplicity, the amplitude and phase correction terms $A\left(\mathbf{m},\widehat{\mathbf{m}},\widehat{\mathbf{h}}\right)\frac{\partial}{\partial t}$ are omitted in the sum (10).

The new time-shift imaging condition can be implemented in Kirchhoff imaging using a slight modification of equation (10) that is equivalent to equations (6) and (8):

$$\mathbf{R}\left(\mathbf{m},\tau\right)=\sum_{\widehat{\mathbf{m}},\widehat{\mathbf{h}}}\widehat{\mathbf{u}}\left[\widehat{\mathbf{m}},\widehat{\mathbf{h}},T_s\left(\mathbf{m},\widehat{\mathbf{m}}-\widehat{\mathbf{h}}\right)+T_r\left(\mathbf{m},\widehat{\mathbf{m}}+\widehat{\mathbf{h}}\right)+2\tau\right]\ . \qquad (11)$$

MOVEOUT ANALYSIS

We can use the Kirchhoff formulation to analyze the moveout behavior for time-shift imaging condition in the simplest case of a flat reflector in a constant-velocity medium. Let s_0 and z_0 represent the true slowness and reflector depth, and s and z stand for the corresponding quantities used in migration. An image is formed when the Kirchoff stacking curve $t(\hat{h})=2s\sqrt{z^2+\hat{h}^2}+2\tau$ touches the true reflection response $t_0(\hat{h})=2s_0\sqrt{z_0^2+\hat{h}^2}$ (Figure 1). Eliminating $\hat{h}$ from the conditions $t(\hat{h})=t_0(\hat{h})$ and $t'(\hat{h})=t_0'(\hat{h})$, we find that the reflection response maps into two images in the $\{z,\tau\}$ space. The first image is a straight line

$$z(\tau)=\frac{z_0\,s_0+\tau}{s}\ , \qquad (12)$$

and the second image is a segment of the second-order curve

$$z(\tau)=\sqrt{z_0^2+\frac{\tau^2}{s^2-s_0^2}}\ . \qquad (13)$$

Applying a slant-stack transformation with $z=z_1+\nu\tau$ turns line (12) into a point $\{z_0\,s_0/s,1/s\}$ in the $\{z_1,\nu\}$ space, while curve (13) turns into the curve

$$z_1(\nu)=z_0\sqrt{1+\nu^2\left(s_0^2-s^2\right)}\ . \qquad (14)$$

The curvature of the $z_1(\nu)$ curve at $\nu=0$ is a clear indicator of the migration velocity errors.

By contrast, the moveout shape $z(h)$ appearing in wave-equation migration with the lateral-shift imaging condition is (Bartana et al., 2005)

$$z(h)=s_0\sqrt{\frac{z_0^2}{s^2}+\frac{h^2}{s^2-s_0^2}}\ . \qquad (15)$$

After the slant transformation $z=z_1+h\tan\theta$, the moveout curve (15) turns into the curve

$$z_1(\theta)=\frac{z_0}{s}\sqrt{s_0^2+\tan^2\theta\left(s_0^2-s^2\right)}\ , \qquad (16)$$

which is applicable for velocity analysis. A formal connection between ν-parameterization in equation (14) and θ-parameterization in equation (16) is given by

$$\tan^2\theta=s^2\nu^2-1\ . \qquad (17)$$

Curves of shape (14) and (16) are plotted on top of the experimental moveouts in Figures 3 and 5, respectively.

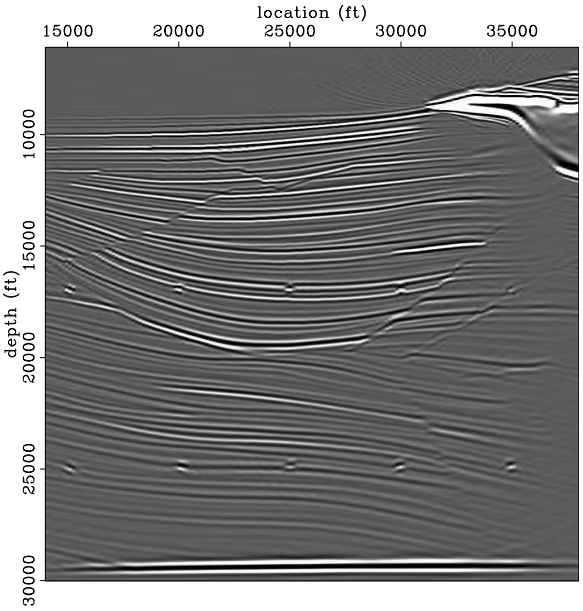

Figure 6: Sigsbee 2A image with time-shift imaging ($\tau=0$).

EXAMPLES

Our first example corresponds to a flat reflector in a constant velocity medium. The synthetic data are imaged using shot-record wavefield extrapolation migration. Figures 2 and 4 show common-offset gathers for three different migration slownesses s, one of which is equal to the modeling slowness s_0. For the time-offset CIGs imaged with correct slowness, Figure 2, the energy is distributed along a line with a slope equal to the local velocity at the reflector position, but it spreads around this region when the slowness is wrong. Slant-stacking produces the images in Figure 3. For the space-shift CIGs imaged with correct slowness, Figure 4, the energy is focused at zero offset, but it spreads in a region of offsets when the slowness is wrong. Slant-stacking produces the images in Figure 5.

In our second example, we use the Sigsbee 2A synthetic model (Paffenholz et al., 2002). Figure 6 shows the image created by shot-record migration using the time-shift imaging condition ($\tau=0$). Figures 7 and 9 show common-image gathers at 25000 ft, for correct and incorrect velocity, respectively. The left panels show a portion of the image at zero offset ($\mathbf{h}=0$ or $\tau=0$). The middle panels correspond to the space-shift imaging condition, and the right panels correspond to the time-shift imaging condition. Figures 8 and 10 show the same common-image gathers after slant-stack and conversion to pseudo-angle using equation (17). All reflections are either flat for correct velocity, or bend indicating velocity inaccuracy.

CONCLUSIONS

We introduce a new imaging condition based on time-shifts between source and receiver wavefields. This method is applicable to both Kirchhoff and wave-equation migration and produces common-image gathers that indicate velocity errors. In wave-equation imaging, time-shift imaging is more efficient than space-shift imaging, since it only involves a phase shift applied prior to the usual imaging cross-correlation. More research is needed to investigate how this new information can be used for velocity and amplitude analysis.

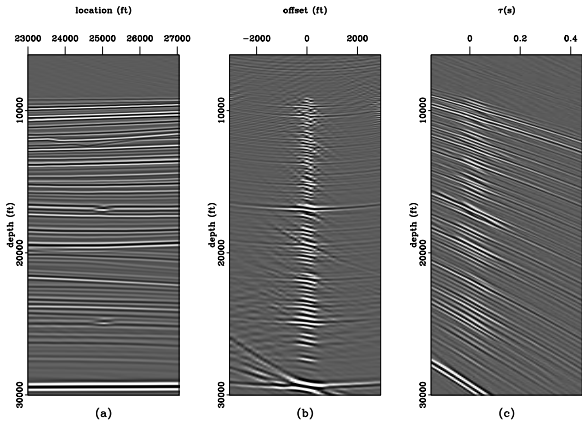

Figure 7: Image zoom (a) and offset gathers for space-shift (b) and time-shift (c). Migration with correct velocity.

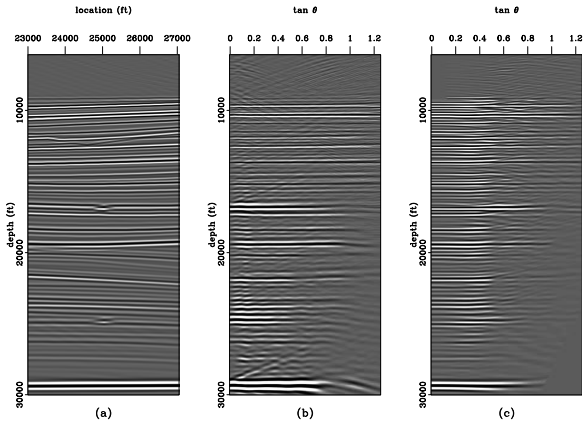

Figure 8: Image zoom (a) and angle gathers for space-shift (b) and time-shift (c). Migration with correct velocity.

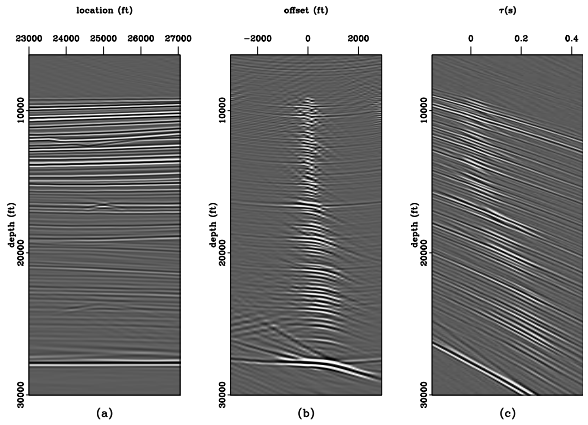

Figure 9: Image zoom (a) and offset gathers for space-shift (b) and time-shift (c). Migration with incorrect velocity.

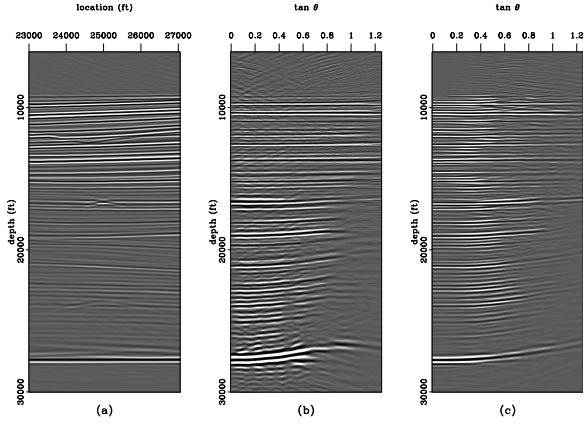

Figure 10: Image zoom (a) and angle gathers for space-shift (b) and time-shift (c). Migration with incorrect velocity.

REFERENCES

Bartana, A., Kosloff, D., and Ravve, I., 2005, On angle-domaina common-image gathers by wavefield continuation methods: Geophysics, submitted.

Biondi, B., and Symes, W. W., 2004, Angle-domain common-image gathers for migration velocity analysis by wavefield-continuation imaging: Geophysics, **69**, 1283–1298.

de Bruin, C. G. M., Wapenaar, C. P. A., and Berkhout, A. J., 1990, Angle-dependent reflectivity by means of prestack migration: Geophysics, **55**, 1223–1234.

Claerbout, J. F., 1985, Imaging the Earth's Interior: Blackwell Scientific Publications.

Mosher, C., and Foster, D., 2000, Common angle imaging conditions for prestack depth migration *in* 70th Ann. Internat. Mtg. Soc. of Expl. Geophys., 830–833.

Paffenholz, J., McLain, B., Zaske, J., and Keliher, P., 2002, Subsalt multiple attenuation and imaging: Observations from the Sigsbee2B synthetic dataset *in* 72nd Ann. Internat. Mtg. Soc. of Expl. Geophys., 2122–2125.

Prucha, M., Biondi, B., and Symes, W., 1999, Angle-domain common image gathers by wave-equation migration *in* 69th Ann. Internat. Mtg. Soc. of Expl. Geophys., 824–827.

Rickett, J. E., and Sava, P. C., 2002, Offset and angle-domain common image-point gathers for shot-profile migration: Geophysics, **67**, 883–889.

Sava, P., and Fomel, S., 2005, Coordinate-independent angle-gathers for wave equation migration *in* 75th Ann. Internat. Mtg. Soc. of Expl. Geophys.

Sava, P. C., and Fomel, S., 2003, Angle-domain common-image gathers by wavefield continuation methods: Geophysics, **68**, 1065–1074.

Soubaras, R., 2003, Angle gathers for shot-record migration by local harmonic decomposition *in* 73rd Ann. Internat. Mtg. Soc. of Expl. Geophys., 889–892.

Stolk, C., and Symes, W., 2002, Artifacts in Kirchhoff common image gathers *in* 72nd Ann. Internat. Mtg. Soc. of Expl. Geophys., 1129–1132.

Xie, X., and Wu, R., 2002, Extracting angle domain information from migrated wavefield *in* 72nd Ann. Internat. Mtg. Soc. of Expl. Geophys., 1360–1363.